ACS APPLIED POLYMER MATERIALS

pubs.acs.org/acsapm Article

Ester-Modified Dicyanoaniline Derivative with Tunable Afterglow via Polymer Matrix and Thermal Annealing for Dynamic Encryption and Iron(III) Detection

Jianqiang Han, Haoqun Wu, Huan Yang, Lei Ma,* and Yongtao Wang*

Cite This: https://doi.org/10.1021/acsapm.5c04339 Read Online

ACCESS | Metrics & More | Article Recommendations | Supporting Information

ABSTRACT: This study develops a pure organic phosphor, Me-ADBD, which exhibits dual-state emission by combining thermally activated delayed fluorescence (TADF) and room-temperature phosphorescence (RTP). Through a host−guest doping strategy using PMMA and PVA matrices, the phosphorescence emission wavelength, TADF/*RTP* intensity ratio, and afterglow duration are effectively tuned. Optimized 1% Me-ADBD@PMMA and 1% Me-ADBD@PVA films achieve afterglow durations of 6 and 7 s, respectively. Thermal treatment at 150 °C further enhances the performance of PVA-based films, extending the afterglow to 10 s and improving water resistance. The material also demonstrates sensitive Fe^{3+} detection based on afterglow quenching, enabling instrument-free visual analysis. Theoretical calculations reveal that a small singlet−triplet energy gap (ΔE_{ST2} = 0.51 eV) and strong spin−orbit coupling facilitate efficient TADF. Finally, multilevel anticounterfeiting and dynamic information encryption are constructed. This work provides insights into designing versatile organic phosphors for advanced optical applications.

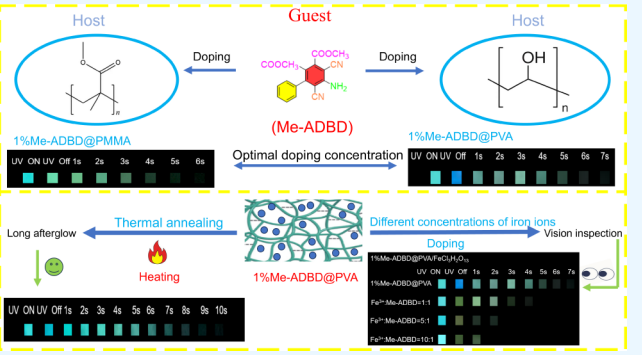

KEYWORDS: *Room temperature phosphorescence, Thermally activated delayed fluorescence, Iron(III)-detection, Encryption, Host−guest doping*

1. INTRODUCTION

Organic dual-state emission (DSE) materials exhibiting both thermally activated delayed fluorescence (TADF) and room-temperature phosphorescence (RTP) have garnered significant attention due to their potential in advanced optoelectronic applications, such as anticounterfeiting, sensing, and information encryption.[1−9] TADF, which relies on efficient reverse intersystem crossing (RISC) from triplet to singlet states via thermal activation, has revolutionized the organic light-emitting diode (OLED) design by enabling full exciton utilization without heavy metals. Seminal contributions, such as the carbazolyl dicyanobenzene emitters reported by Adachi et al.,[10] established donor−acceptor molecular architectures that minimize singlet−triplet energy gaps (ΔE_{ST}) to promote RISC. Subsequent advances, including the role of hydrogen bonding in enhancing TADF efficiency as explored by Bryce et al.[11] and the systematic design of donor−acceptor systems elucidated by Brédas et al.,[12] have further expanded the mechanistic understanding and material scope of TADF emitters. Integrating such TADF components with RTP in a single system enables DSE materials with long-lived afterglow, offering unique advantages for time-resolved visual detection and dynamic information display.[13−16] However, achieving efficient and tunable RTP in pure organic systems remains challenging due to issues such as nonradiative decay, triplet exciton quenching by molecular motions, and sensitivity to oxygen.[17] Host−guest doping strategies have emerged as an effective approach to immobilize phosphors within rigid polymer matrices, suppressing vibrational dissipation and shielding against oxygen.[18−23] Despite these advances, there is a growing need to further enhance host−guest interactions through simple and scalable methods to improve phosphorescence performance[24−28] and enable broader practical applications.[29,30]

In this study, we designed a multifunctional organic molecule, Me-ADBD, incorporating ester, cyano, and amino functional groups to strengthen host−guest interactions and facilitate metal ion detection (Scheme 1).[31−39] The presence of multiple coordination sites was expected to promote rigidification within polymer matrices such as PMMA and PVA and

Received: December 15, 2025
Revised: March 18, 2026
Accepted: March 19, 2026

Scheme 1. Synthesis Route and Reaction Mechanism of Me-ADBD

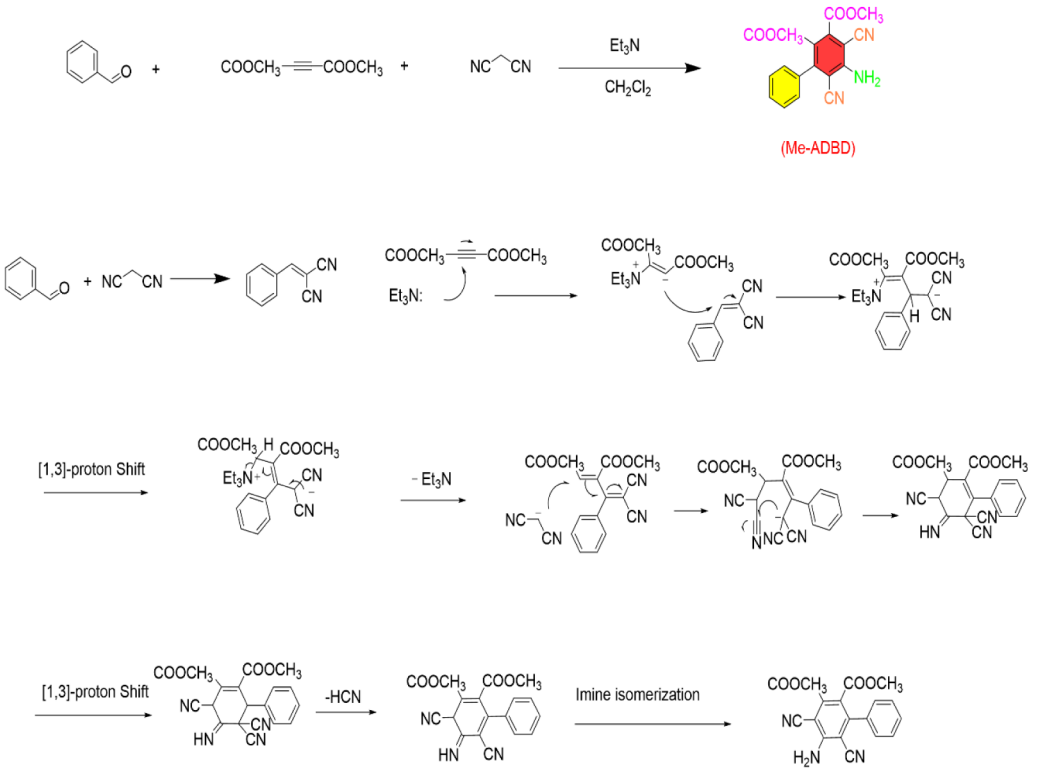

provide binding affinity toward metal ions, enabling visual detection based on afterglow modulation.[40−43] There are both electron donor and electron acceptor groups in the dicyanoaniline structural unit, with an amino group as the donor group, two cyano groups, and ester groups as acceptors, and a biphenyl skeleton as the π bridge, endowing Me-ADBD with intramolecular charge transfer (ICT) properties.[44] The molecular structure and purity of compound Me-ADBD were characterized and confirmed by using ^{1}H NMR, ^{13}C NMR, HR-MS, and HPLC (Figures S1−S4). More importantly, dicyanoaniline derivatives were repeatedly confirmed by our research group to possess DSE characteristics.[40] Thereby, Me-ADBD was expected to achieve efficient TADF and RTP emissions, tunable afterglow, and ion-detection ability through matrix selection, doping-concentration optimization, and heat treatment.

Leveraging these structural features, we systematically investigated the photophysical behavior of Me-ADBD in different polymers. The results demonstrate that PVA's robust hydrogen-bonding network significantly prolongs the phosphorescence lifetime compared to PMMA.[45] Moreover, thermal annealing further induces enhancement of afterglow duration[46,47] and water resistance.[48] The material also serves as a sensitive probe for Fe^{3+} detection, where the afterglow quenching provides a visible readout without specialized instruments. These findings highlight the potential of simple chemical modifications and matrix interactions to optimize the RTP properties and expand the functionality of organic phosphors in real-world applications.

2. EXPERIMENTAL SECTION

Me-ADBD was prepared by a one-step method. Detailed synthetic procedures, structural characterization, and host−guest doping details are available in the Supporting Information.

3. RESULTS AND DISCUSSION

3.1. Photophysical Properties

First, the UV−vis absorption and fluorescence emission spectra of Me-ADBD were examined in different solvents (10^{-5} M). The absorption maxima of Me-ADBD undergo only a modest red shift (10−15 nm) upon transitioning from nonpolar *n*-hexane to polar DMSO, which suggests a relatively weak ground-state dipole moment. By contrast, the emission maxima of Me-ADBD exhibit a far more pronounced bathochromic shift (416 → 472 nm, $\Delta\lambda$ = 56 nm) across the same solvent series (Figure 1b and Figure S5). This dramatic emission red shift unveils a significantly enhanced dipole moment in the excited state and provides compelling evidence of intramolecular charge transfer (ICT) character. The emission spectrum reveals a striking contrast between fluorescence (438 nm) and phosphorescence (531 nm) in glassy THF at 77 K. Switching on/off a 365 nm UV lamp reveals that the glassy solution of Me-ADBD exhibits blue fluorescence and a bright, long-lived green afterglow separately, lasting for 13 s (Figure S6). The long-lived afterglow phenomenon confirms the phosphorescent nature of Me-ADBD. Notably, in addition to the main phosphorescence peak, a weak shoulder peak located within the fluorescence emission region is also detected in the phosphorescence emission spectrum (Figure 1c). Furthermore, variable-temperature phosphorescence spectra reveal that there are two emission peaks (456 and 545 nm) at 277 K in glassy DMSO, whereas solely a single phosphorescence peak (530 nm) is observed at 77 K. This discrepancy strongly supports that Me-ADBD has dual-state emission characteristics involving both TADF (456 nm) and RTP (545 nm).

3.2. Host−Guest Doping

Me-ADBD can exhibit a bright, long-lived afterglow in glassy solutions, but its solid powders fail to yield a visible afterglow

https://doi.org/10.1021/acsapm.5c04339
ACS Appl. Polym. Mater. XXXX, XXX, XXX−XXX

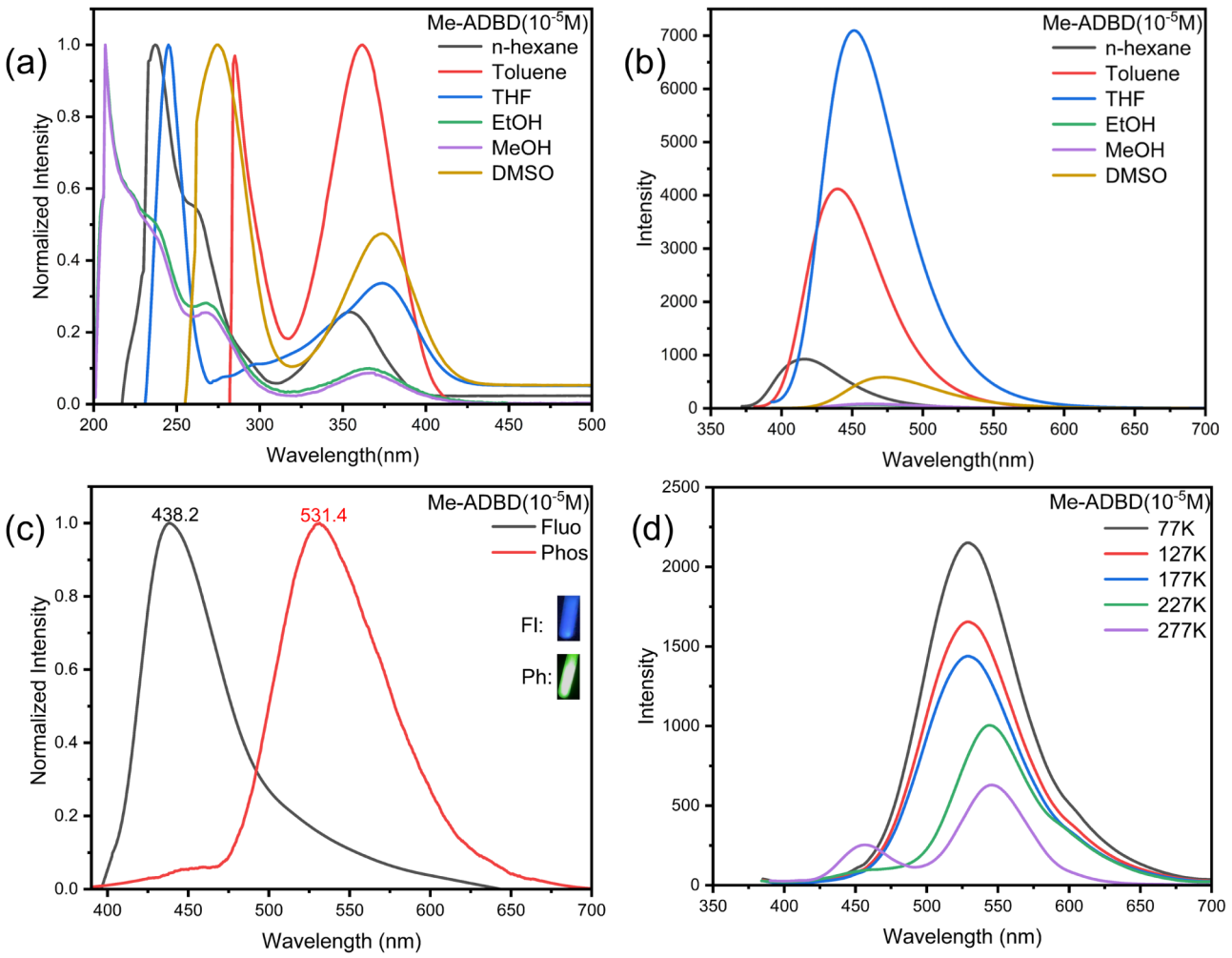

Figure 1. (a) Normalized UV−vis absorption spectra of Me-ADBD in different solvents (10^{-5} M). (b) Fluorescence emission spectra of compound Me-ADBD in different solvents (10^{-5} M). (c) Fluorescence and phosphorescence spectra of Me-ADBD in a glassy THF solution (10^{-5} M) at 77 K. (d) Temperature-variable phosphorescence spectra of Me-ADBD in a glassy DMSO solution (10^{-5} M).

at room temperature, which is primarily attributed to intensified molecular motions (vibrations/rotations). The host−guest doping strategy not only effectively suppresses molecular vibrations and rotations but also eliminates phosphorescence quenching caused by molecular aggregation. More importantly, this approach can construct an oxygen-free, rigid microenvironment for phosphorescent chromophores, simultaneously addressing the dual challenges of molecular motion suppression and oxygen quenching, thereby providing an optimal condition for efficient and stable phosphorescent emissions. First, three doping systems named 0.1% Me-ADBD@PMMA, 1% Me-ADBD@PMMA, and 5% Me-ADBD@PMMA were constructed and optimized at mass ratios from 0.1% to 5% between Me-ADBD and PMMA. By contrast, the 1% Me-ADBD@PMMA film exhibits the longest afterglow duration (6 s) and the strongest phosphorescence emission (Figure S7), whose fluorescence and RTP emission maxima are 437 and 522 nm, respectively, corresponding to ΔE_{ST} of 0.46 eV. Similar to the THF glassy solution of Me-ADBD, the 1% Me-ADBD@PMMA film also gives a shoulder peak at 441 nm in the RTP spectrum. Temperature-variable phosphorescence spectra of the 1% Me-ADBD@PMMA film further confirm dual-state emissions with RTP and TADF. As shown in Figure 2c, TADF emission of 1% Me-ADBD@PMMA can be detected when the temperature increases to 234 K, and as the temperature further increases to 303 K, the emission intensity further enhances, presenting typical TADF features. Moreover, the 1% Me-ADBD@PMMA film shows a longer lifetime for TADF (657.1 ms) than RTP (555.3 ms), which is inconsistent with the triplet−triplet annihilation mechanism (TTA), illustrating that dual-state emissions originate from the Me-ADBD skeleton itself. Notably, with increasing temperature, the phosphorescence maxima undergo continuous red shifts, likely due to enhanced nonradiative transitions at higher temperatures (Figure 2c).

To further investigate the regulatory effects of different polymer matrices on phosphorescence properties such as emission wavelength, intensity ratio of TADF to RTP, and phosphorescence lifetime, PVA was subsequently selected as the doping matrix. Compared with PMMA, the PVA molecular chain contains abundant hydroxyl groups. PVA is used as a host matrix due to its robust intermolecular hydrogen-bonding network, which not only effectively suppresses molecular motions of phosphorescent molecules but also forms a compact physical barrier to isolate oxygen, thereby providing a more stable microenvironment for long-lived phosphorescence emissions. To optimize the RTP performance at different doping concentrations, 0.1% Me-ADBD@PVA, 1%

https://doi.org/10.1021/acsapm.5c04339
ACS Appl. Polym. Mater. XXXX, XXX, XXX−XXX

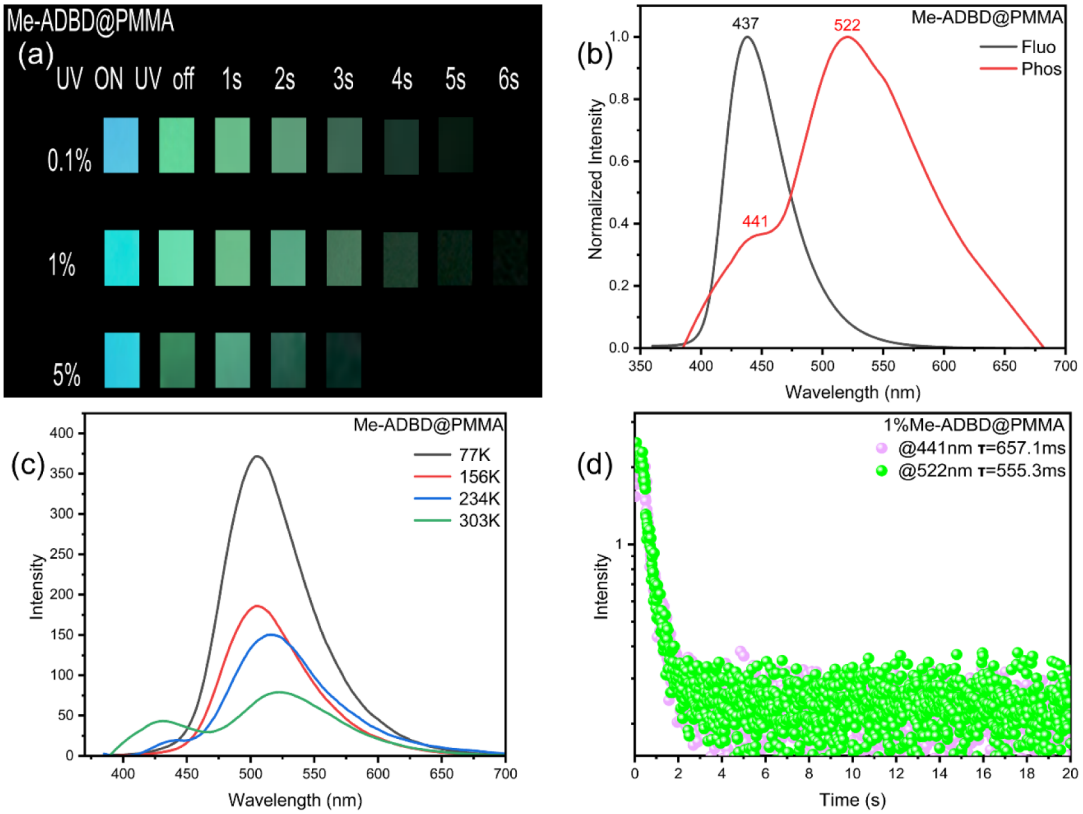

Figure 2. (a) Digital photos of Me-ADBD in PMMA at doping concentrations of 0.1%, 1%, and 5% (λ_{ex} = 365 nm). (b) The normalized fluorescence and phosphorescence spectra of the 1% Me-ADBD@PMMA film. (c) Temperature-variable phosphorescence spectra of the 1% Me-ADBD@PMMA film. (d) Phosphorescence lifetime decay curves of the 1% Me-ADBD@PMMA film at 441 and 522 nm.

Me-ADBD@PVA, and 5% Me-ADBD@PVA films were prepared. As shown in Figure 3a, the 1% Me-ADBD@PVA film shows the best phosphorescence performance based on a comprehensive evaluation of phosphorescence intensity (Figure S8) and afterglow duration. Compared with the 1% Me-ADBD@PMMA film, the 1% Me-ADBD@PVA film shows a longer afterglow duration (7 s) but displays a different afterglow color. Furthermore, the fluorescence and RTP emission maxima of the 1% Me-ADBD@PVA film are 439 and 493 nm in turn (Figure 3b), presenting significant blue shifts compared to those of the 1% Me-ADBD@PMMA film. Meanwhile, the dual-band emission profile (437 and 493 nm) observed in the phosphorescence spectrum (Figure 3b), combined with the temperature-dependent phosphorescence spectral behavior (Figure 3c), provides clear evidence for the dual-state characteristics of the 1% Me-ADBD@PVA film, demonstrating the coexistence of TADF and RTP. The TADF and RTP lifetimes of the 1% Me-ADBD@PVA film are 560.4 and 711.3 ms, respectively, but different TADF and RTP lifetimes do not yield obvious dynamic afterglow. Importantly, the 1% Me-ADBD@PVA film exhibits a significantly enhanced intensity ratio between TADF and RTP emissions compared with that of the 1% Me-ADBD@PMMA film. Obviously, the distinct afterglow colors between the 1% Me-ADBD@PMMA and 1% Me-ADBD@PVA films are due to the altered TADF and RTP emission maxima, as well as the TADF/RTP intensity ratio. The comparison reveals that the ΔE_{ST} of the 1% Me-ADBD@PVA film is 0.16 eV lower than that of the 1% Me-ADBD@PMMA film. This narrowing of ΔE_{ST} thermodynamically favors the reverse intersystem crossing (RISC) process from the triplet (T_1) to the singlet (S_1) excited state, thereby intensifying the TADF emission and enhancing the TADF/RTP intensity ratio of the 1% Me-ADBD@PVA film.

Me-ADBD contains two methyl benzoate structural units. Through thermal annealing, Me-ADBD is expected to anchor directly onto PVA molecular chains, further strengthening the host−guest interactions. To systematically investigate the above conjecture, 1% Me-ADBD@PVA films are heated for 30 min at varying temperatures. As shown in Figure 4, when the heat treatment temperature is maintained within the range of 60−120 °C, the afterglow durations of 1% Me-ADBD@PVA films exhibit no significant variation. When the temperature is elevated to 150 °C, the afterglow duration of the 1% Me-ADBD@PVA film increases markedly (10 s). This enhancement can be ascribed to two synergistic mechanisms: (1) The moderately elevated temperature promotes the ordered arrangement of molecular chains and strengthens the compactness of the hydrogen-bonding network within the polymer matrix, thereby more effectively suppressing nonradiative transitions of the phosphorescent molecules; (2) This temperature may have reached the cross-linking threshold, achieving the anchoring of the phosphorescent chromophore to the PVA chains, further stabilizing the triplet excitons and reducing energy dissipation through nonradiative pathways. However, the afterglow duration of the 1% Me-ADBD@PVA film decreases instead when the temperature is further increased to 180 °C. This decline is probably due to excessive cross-linking or thermal degradation of the polymer chains disrupting the rigid and oxygen-free microenvironment essential for triplet excitons. Subsequently, the time-resolved delayed decay curves, fluorescence, and phosphorescence spectra of the 1% Me-ADBD@PVA film treated at 150 °C

https://doi.org/10.1021/acsapm.5c04339
ACS Appl. Polym. Mater. XXXX, XXX, XXX−XXX

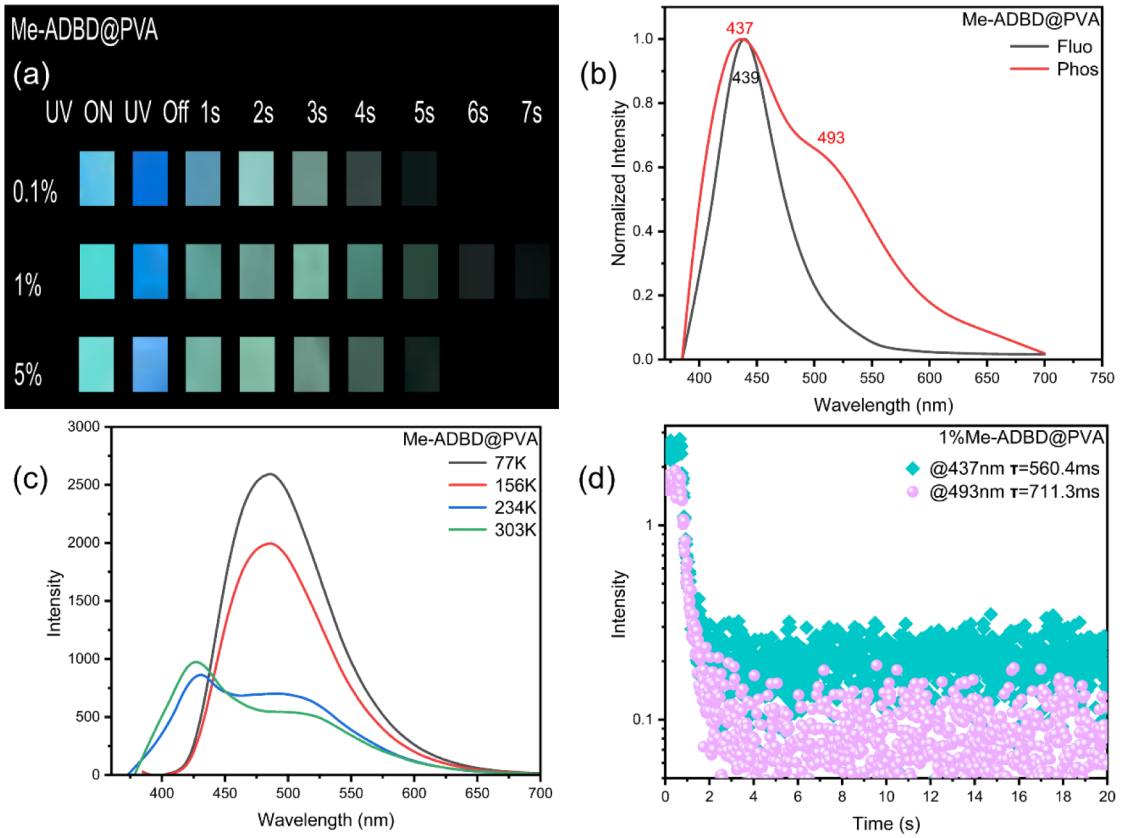

Figure 3. (a) Digital photos of Me-ADBD in PVA at doping concentrations of 0.1%, 1%, and 5% (λ_{ex} = 365 nm). (b) The normalized fluorescence and phosphorescence spectra of the 1% Me-ADBD@PVA film. (c) Temperature-variable phosphorescence spectra of the 1% Me-ADBD@PVA film. (d) Phosphorescence lifetime decay curves of the 1% Me-ADBD@PVA film at 437 and 493 nm.

(1% *t*-Me-ADBD@PVA film) are measured. Compared to the 1% Me-ADBD@PVA film, fluorescence emission maxima of the 1% *t*-Me-ADBD@PVA film remain basically stable, while its phosphorescence emission maxima show blue shifts of 7 nm, resulting in a reduced ΔE_{ST}. Furthermore, TADF and RTP of the 1% *t*-Me-ADBD@PVA film are 740.1 and 1080.3 ms, respectively, which are 1.13-fold and 1.95-fold longer than those of the 1% Me-ADBD@PMMA film, and 1.32-fold and 1.52-fold longer than those of the 1% Me-ADBD@PVA film. According to the reported literature,[49] the following formulas are adopted. $\tau_{TADF} \approx 1/(K_{RISC} + K_P)$; $K_P \approx 1/\tau_{P_{77K}}$; $K_{RISC} = 1/\tau_{TADF} - K_P$. From the above formula, the phosphorescence radiative rate (K_P) and reverse intersystem crossing rate (K_{RISC}) were obtained, which are 0.75 and 0.6 s^{-1}, respectively (Figure 4, Figure S9 and Table S1). Such close K_P and K_{RISC} are responsible for the 1% *t*-Me-ADBD@PVA film simultaneously exhibiting long-lived RTP and TADF. For the 1% *t*-Me-ADBD@PVA film, the intensity ratio between TADF and RTP is approximately 0.8, and the dynamic afterglow from blue to green can be observed. To elucidate the intrinsic mechanism of thermal treatment, the Fourier-transform infrared spectroscopy (FTIR) of the 1% Me-ADBD@PVA film treated at 60 and 150 °C is systematically investigated. For the 1% Me-ADBD@PVA film treated at 60 °C, the broad absorption peak observed around 3296 cm^{-1} is assigned to the O−H stretching vibration of PVA, indicating the presence of intermolecular hydrogen bonding. The peaks at 2918 cm^{-1} and 2852 cm^{-1} correspond to the asymmetric and symmetric stretching vibrations of the methyl (Me) groups in COOMe, respectively. The peak at 1732 cm^{-1} is attributed to the C═O stretching vibration of COOMe, while the skeletal vibrations of the benzene are located at 1575 cm^{-1} and 1541 cm^{-1}. In contrast, the C═O stretching frequency shifts from 1732 cm^{-1} to 1716 cm^{-1} after 150 °C treatment. At high temperatures, carbonyl of ester prefers a more stable conformer (in between s-trans vs s-cis), which induces a red shift in the C═O stretching vibration. Additionally, the formation of new covalent bonds between PVA and Me-ADBD through cross-linking can also trigger a red shift in the C═O stretching frequency. Moreover, the vibration intensity of the benzene ring skeleton (1575/1541 cm^{-1}) weakens, reflecting a significant alteration in the electronic environment around the benzene ring. Meanwhile, the O−H stretching vibration peak of PVA shifts slightly from 3296 cm^{-1} to 3288 cm^{-1}, indicating enhanced intermolecular hydrogen bonds. Collectively, the treatment at 150 °C induces conformation transition/cross-linking, the rearrangement and redistribution of phosphorescent chromophores, and the enhanced intermolecular hydrogen bonds, leading to a significant improvement of afterglow duration. To visually compare the impact of heat treatment at 60 °C versus 150 °C, two 1% Me-ADBD@PVA films were immersed in 2 mL of deionized water for 5 h (Figure S10). In contrast, the 1% Me-ADBD@PVA film treated at 60 °C exhibits complete dissolution, while the 1% Me-ADBD@PVA film treated at 150 °C retained >60% of its original area, demonstrating significantly enhanced water resistance. This stark contrast provides direct experimental evidence that thermal annealing at 150 °C induces covalent cross-linking between PVA and Me-ADBD.

https://doi.org/10.1021/acsapm.5c04339
ACS Appl. Polym. Mater. XXXX, XXX, XXX−XXX

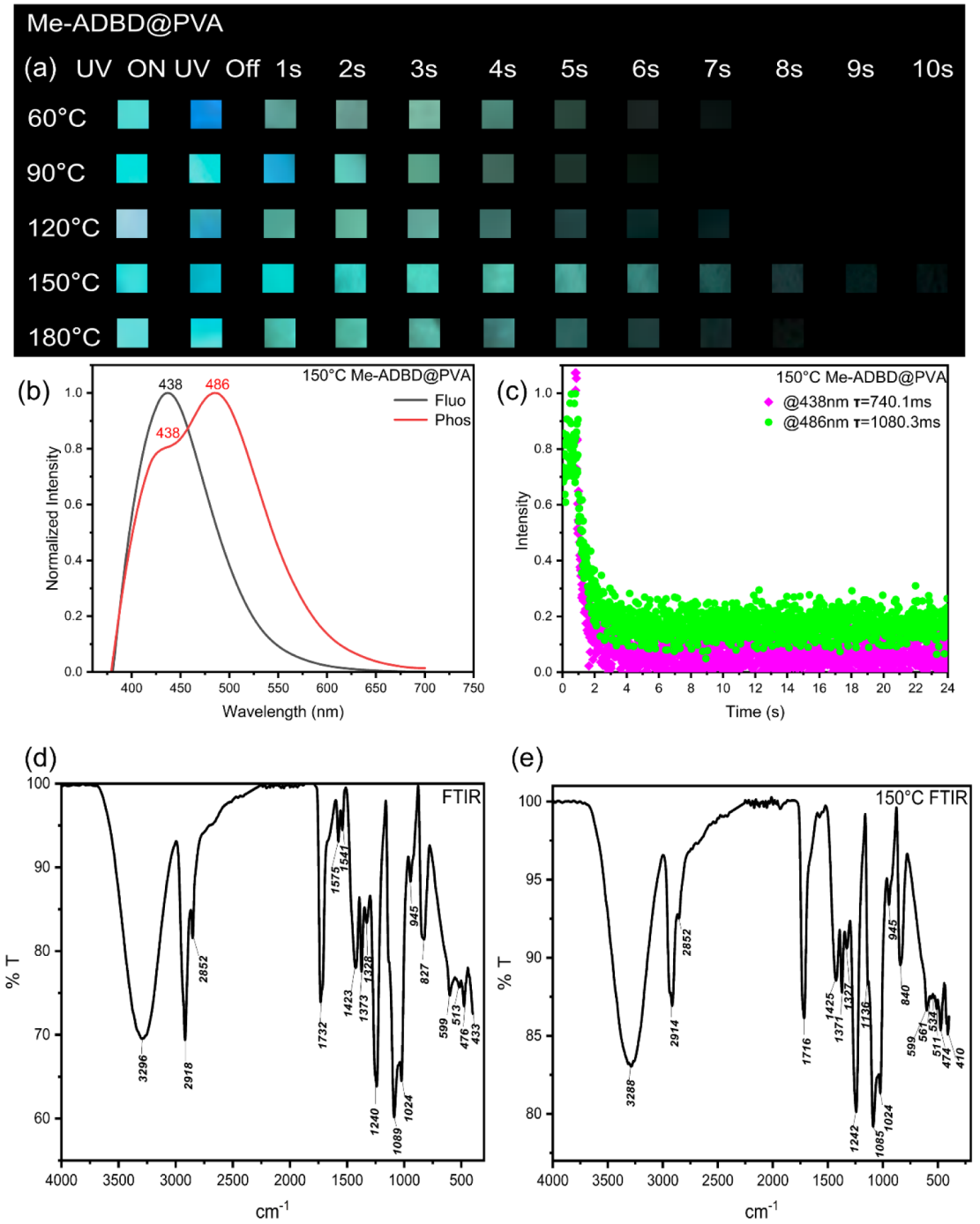

Figure 4. (a) Digital photos of the 1% Me-ADBD@PVA film after heat treatment at 60−180 °C for 30 min (λ_{ex} = 365 nm). (b) Normalized fluorescence and phosphorescence spectra and (c) phosphorescence lifetime decay curves of the 1% Me-ADBD@PVA film after heat treatment (150 °C). (d−e) Infrared spectra of the 1% Me-ADBD@PVA film before/after heat treatment (150 °C).

3.3. Ion Detection

Research on pure organic room-temperature phosphorescence materials for metal ion detection is still in its infancy, yet their unique advantages hold significant scientific importance and practical potential. Visualization-based detection through afterglow duration variations enables qualitative or even semiquantitative analysis of metal ions without relying on expensive spectrometers or fluorimeters. Different metal ions induce distinct modulation effects on the afterglow duration, creating unique "temporal fingerprints" for selective identification. Me-ADBD with a long-lived RTP serves as the core probe molecule. Its multiple functional groups (e.g., cyano, ester, and amino groups) are expected to interact with metal ions, altering the afterglow lifetime and providing a sufficient temporal window for visualized detection. Thereby, a series of doping films are constructed, where Me-ADBD and metal ions are mixed at a 1:10 molar ratio. The results showed that Ba^{2+}, Ca^{2+}, and Zn^{2+} produced almost negligible influence on afterglow duration, while Cd^{2+}, Mn^{2+}, Mg^{2+}, Cu^{2+}, and Ni^{2+} shortened the afterglow duration from 7 s to 4−5 s. In contrast, Fe^{3+} demonstrates the most pronounced quenching effect, leading to a significant reduction in the afterglow

https://doi.org/10.1021/acsapm.5c04339
ACS Appl. Polym. Mater. XXXX, XXX, XXX−XXX

lifetime. As speculation, the partially filled 3d orbital of Fe^{3+} enables intense competition with excited states of Me-ADBD, effectively depleting the excited-state energy through strong electron coupling or energy transfer. Furthermore, the influence of iron ion concentration on the afterglow duration of 1% Me-ADBD@PVA was investigated. As shown in Figure 5b, as the molar ratio of Fe^{3+} to Me-ADBD continuously decreases from 10:1 to 1:1, the afterglow duration of the material exhibits a significant increasing trend. There is a clear negative correlation between the Fe^{3+} concentration and the afterglow duration, which facilitates the advancement of Fe^{3+} detection from qualitative analysis to quantitative detection. By correlating the afterglow duration with specific metal ions, this approach establishes a simple, cost-effective, and instrument-free platform for visualized metal ion detection.

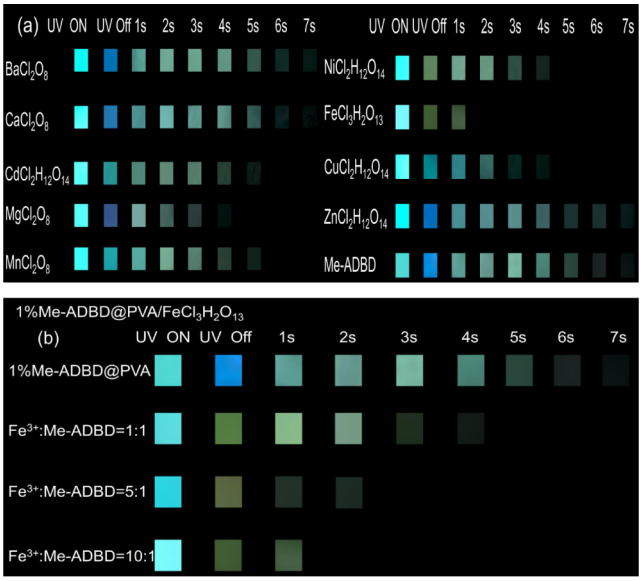

Figure 5. (a) Digital photos of the 1% Me-ADBD@PVA film before and after treatment with different perchlorates. (b) Digital photos of the 1% Me-ADBD@PVA film before and after treatment with different equivalents of iron perchlorate.

3.4. Theoretical Calculation

In this work, based on the ORCA 6.0.0 software package, the structure of the compound Me-ADBD was optimized using the ωB97X-D3 functional and the def2-SVP basis set. Based on the optimized ground-state geometry (S_0), the vertical excitation energies of the excited singlet (S) and triplet (T) states were calculated at the ωB97X-D3/Def2-TZVP level. The intersystem crossing (ISC) process of the sample structure was further evaluated by using the ωB97X-D3/Def2-TZVP functional and basis set. Based on the optimized geometry of the S_1 excited state, the electronic structure of the sample and the spin−orbit coupling (SOC) matrix elements between the singlet and triplet states were obtained. The results indicate that the highest occupied molecular orbital (HOMO) and the lowest unoccupied molecular orbital (LUMO) of Me-ADBD are predominantly localized on the dicyanoaniline unit. Even so, Me-ADBD shows a significant intramolecular charge transfer (ICT) characteristic, with the HOMO mainly concentrated on NH_2, the carbon atom attached to NH_2, and the carbon atom attached to an ester group, while the LUMO is primarily distributed on −CN and the ortho/meta carbon atoms of NH_2 (Figure 6). The S_1 state of Me-ADBD was calculated at 3.38 eV with two nearby triplet states: T_1 (1.36 eV, ΔE_{ST} = 1.36 eV, ξ = 0.301 cm^{-1}) and T_2 (0.51 eV, ΔE_{ST2} = 0.51 eV, ξ = 0.237 cm^{-1}). The relatively large ΔE_{ST} suggests inefficient ISC to T_1, whereas the smaller ΔE_{ST2} and moderate ξ indicate a viable pathway for ISC and reverse intersystem crossing (RISC) between S_1 and T_2. The experimental results and theoretical calculations both show that Me-ADBD has a bigger ΔE_{ST}. Therefore, the TADF emission of Me-ADBD should be attributed to the small ΔE_{ST2} and the large ξ between S_1 and T_2.

3.5. Anticounterfeiting and Information Encryption

Leveraging the distinct afterglow colors and durations of 1% Me-ADBD@PMMA and 1% Me-ADBD@PVA films, the process of a peacock fanning and closing its tail feathers was displayed. As shown in Figure 7a, the peacock's wings are composed of the 1% Me-ADBD@PMMA film, while its body is made of the 1% Me-ADBD@PVA film. When the 365 nm UV lamp is turned on, a fully displayed peacock with spread-out tail feathers can be observed. Upon turning off the UV lamp, the peacock's body and wings exhibit blue and green,

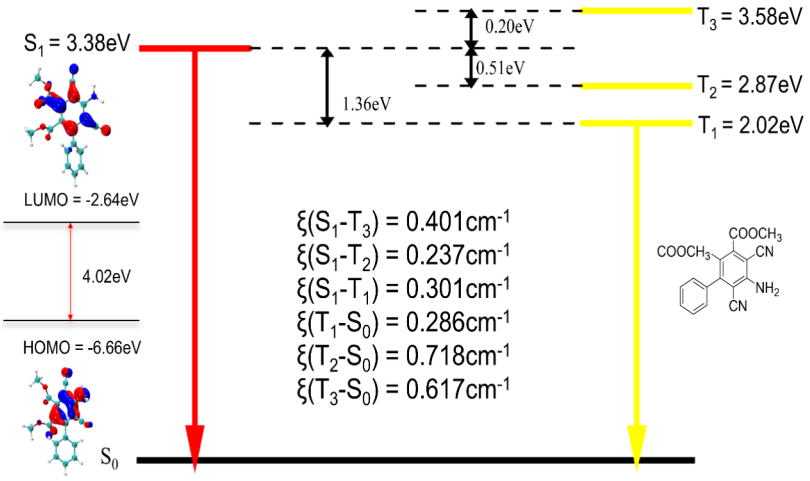

Figure 6. HOMO and LUMO distributions, energy levels, and spin−orbit coupling constants of the Me-ADBD.

https://doi.org/10.1021/acsapm.5c04339
ACS Appl. Polym. Mater. XXXX, XXX, XXX−XXX

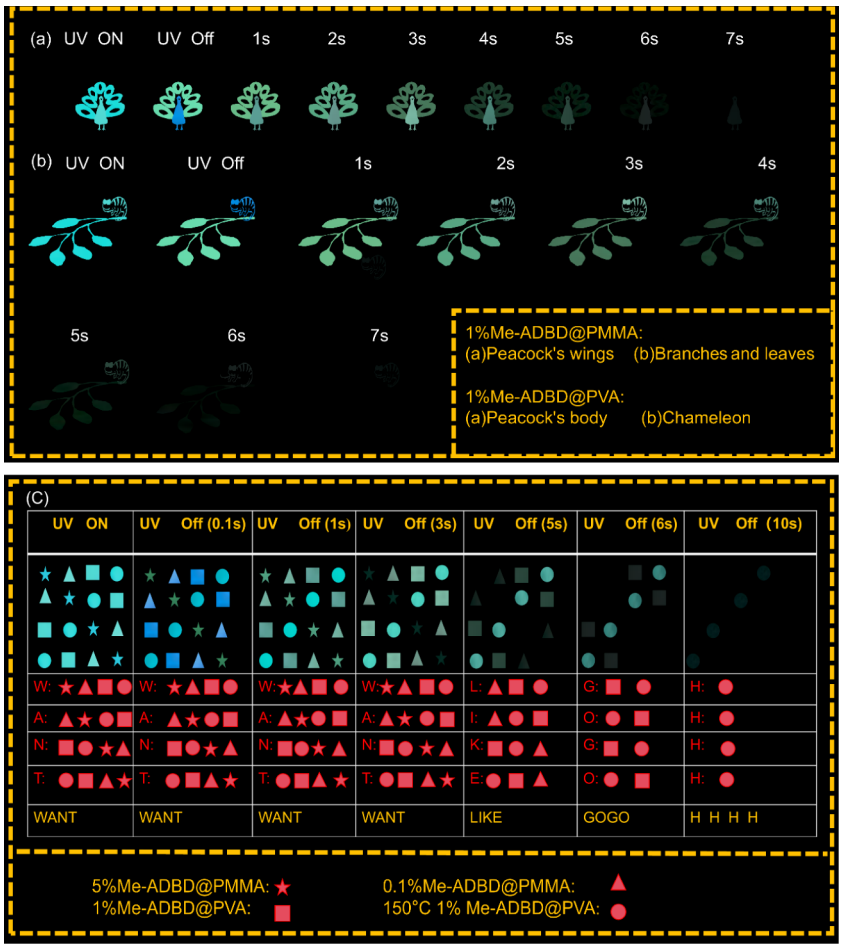

Figure 7. (a–b) Anticounterfeiting photographs prepared by 1% Me-ADBD@PMMA and 1% Me-ADBD@PVA films under ambient conditions; (c) information encryption by 0.1% Me-ADBD@PMMA, 5% Me-ADBD@PMMA, 1% Me-ADBD@PVA, and 1% *t*-Me-ADBD@PVA films.

respectively. Over time, the tail feathers gradually fold in, and by 6 s, the peacock's tail is fully closed. Eventually, the peacock's body completely fades away after 7 s. Figure 7b displays a chameleon perched on foliage, where the leaves and branches are composed of 1% Me-ADBD@PMMA, and the chameleon itself is made of 1% Me-ADBD@PVA. Under 365 nm UV illumination, the entire pattern emits a uniform blue, with the chameleon appearing equally blue. Upon UV cessation, the foliage transitions to green, and the chameleon begins to change color—gradually shifting to green over time. Eventually, as the foliage's luminescence fades, the chameleon also slowly disappears. Figure 7c demonstrates an encryption application based on the varying afterglow durations. The pentagram, equilateral triangle, square, and circle are fabricated by using 5% Me-ADBD@PMMA, 0.1% Me-ADBD@PMMA, 1% Me-ADBD@PVA, and 1% *t*-Me-ADBD@PVA films in turn. The password can be decrypted through the password book (Figure S11). When illuminated under a 365 nm UV lamp, all patterns collectively display the word "WANT". Upon turning off the UV lamp, the "WANT" image persists for the first 3 s to create a decoy effect. From the fourth second onward, the afterglow evolves dynamically. It transitions to "LIKE", "GOGO", and "HHHH" as time progresses. Together, these characters convey our core message: "Follow your heart, give your all, and embrace life with joy!"

4. CONCLUSION

In summary, a dual-emissive organic molecule named Me-ADBD was prepared, whose phosphorescence can be finely regulated through polymer matrix selection, doping concentration, and thermal treatment. The host–guest systems with PMMA and PVA not only suppress nonradiative decay but also adjust the TADF/RTP ratio via rigid microenvironment engineering. Notably, thermal annealing at 150 °C prolonged the afterglow duration and improved water resistance. The material's ability to visually detect Fe^{3+} based on afterglow lifetime offers a low-cost sensing platform. Combined with theoretical insights into the TADF mechanism facilitated by the S_1-T_2 pathway, this study illustrates the potential of molecular and matrix engineering in achieving customizable afterglow properties. The demonstrated applications in dynamic anticounterfeiting and time-resolved encryption underscore the practical value of such smart phosphors in advanced photonic technologies.

■ ASSOCIATED CONTENT

Data Availability Statement

No data was used for the research described in the article.

Supporting Information

The Supporting Information is available free of charge at https://pubs.acs.org/doi/10.1021/acsapm.5c04339.

https://doi.org/10.1021/acsapm.5c04339
ACS Appl. Polym. Mater. XXXX, XXX, XXX–XXX

All experimental details include: the synthesis procedure, preparation of thin-film materials, nuclear magnetic resonance (NMR) spectrum, mass spectrometry (MS), high-performance liquid chromatography (HPLC), phosphorescence afterglow image, fluorescence spectrum and phosphorescence spectrum, life decay curve, contrast image of film immersion, summary table of thin-film photophysical properties, and the codebook (PDF)

AUTHOR INFORMATION

Corresponding Authors

Lei Ma − *Tianjin International Center for Nanoparticles and Nano System, Tianjin University, Tianjin 300072, PR China; Haihe Laboratory for Low Dimensional Electronic Materials, Tianjin 300074, China; Tianjin Key Laboratory of Low Dimensional Electronic Materials and Advanced Scientific Instrumentation, Tianjin 300072, China;* orcid.org/0000-0002-2446-4833; Email: lei.ma@tju.edu.cn

Yongtao Wang − *Guangxi Key Laboratory of Electrochemical and Magneto-Chemical Function Materia, College of Chemistry and Bioengineering, Guilin University of Technology, Guilin 541004, China;* orcid.org/0000-0002-9715-0093; Email: wyt_shzu@163.com

Authors

Jianqiang Han − *Guangxi Key Laboratory of Electrochemical and Magneto-Chemical Function Materia, College of Chemistry and Bioengineering, Guilin University of Technology, Guilin 541004, China*

Haoqun Wu − *Guangxi Key Laboratory of Electrochemical and Magneto-Chemical Function Materia, College of Chemistry and Bioengineering, Guilin University of Technology, Guilin 541004, China*

Huan Yang − *Guangxi Key Laboratory of Electrochemical and Magneto-Chemical Function Materia, College of Chemistry and Bioengineering, Guilin University of Technology, Guilin 541004, China*

Complete contact information is available at: https://pubs.acs.org/10.1021/acsapm.5c04339

Author Contributions

J.H.: Writing − original draft, Methodology, Data curation. H.W.: Writing − original draft, Software. H.Y.: Writing − original draft, Supervision. L.M.: Writing − review and editing, Software. Y.W.: Writing − review and editing, Project administration, Funding acquisition, Conceptualization. J.H and H.W contributed equally to this work.

Notes

The authors declare no competing financial interest.

ACKNOWLEDGMENTS

This work was supported by the National Natural Science Foundation of China (Grant No. 22565012) and the Guangxi Natural Science Foundation (Grant No. 2024GXNSFAA999457).

REFERENCES

(1) Bi, X.; Shi, Y.; Peng, T.; Yue, S.; Wang, F.; Zheng, L.; Cao, Q.-E. Multi-stimuli responsive and multicolor adjustable pure organic room temperature fluorescence-phosphorescent dual-emission materials. *Adv. Funct. Mater.* **2021**, *31* (24), 2101312.

(2) Cai, X.-B.; Liang, D.; Zhang, D.-C.; Jia, J.-H.; Wu, X.-Y.; Lu, C.-Z. Achieving dual emission of thermally activated delayed fluorescence and ultralong room-temperature phosphorescence by controlling excited state dynamics through metal coordination. *Chem. Sci.* **2025**, *16* (22), 9802−9808.

(3) Cardeynaels, T.; Paredis, S.; Danos, A.; Vanderzande, D.; Monkman, A. P.; Champagne, B.; Maes, W. B. [1,2-b: 4,5-b']dithiophene as a weak donor component for push-pull materials displaying thermally activated delayed fluorescence or room temperature phosphorescence. *Dyes Pigm.* **2021**, *186*, 109022.

(4) Chen, K.; Jiang, Y.; Zhu, Y.; Lei, Y.; Dai, W.; Liu, M.; Cai, Z.; Wu, H.; Huang, X.; Dong, Y. Host to regulate the T1−S1 and T1−S0 processes of guest excitons in doped systems to control the TADF and RTP emissions. *J. Mater. Chem. C* **2022**, *10* (32), 11607−11613.

(5) Guo, Y.; Guan, H.; Li, P.; Wang, C.; Wang, Y.; Zhang, J.; Zhao, G. Non-adiabatic conformation distortion charge transfer enables dual emission of thermally activated delayed fluorescence and room temperature phosphorescence. *Spectrochim. Acta, Part A* **2024**, *311*, 124032.

(6) Li, P.; Lv, Q.; Sun, C.; Zhang, P.; Wang, X.; Yin, C.; Pan, Y.; Chen, R. Regulation of TADF and RTP dual emission via internal and external heavy-atom effects. *J. Phys. Chem. Lett.* **2024**, *15* (38), 9787−9794.

(7) Mao, S.; Zhao, Y.; Hong, Y.; Ma, L.; Wang, Y. Tunable thermally activated delayed fluorescence and room-temperature phosphorescence emissions, white and red long afterglow driven by host−guest doping and substituent electronic effects. *ACS Appl. Mater. Interfaces* **2025**, *17* (42), 58669−58680.

(8) Su, N.; Wang, J.; Yang, Y.; Yan, Z.; Zhou, L.; Zheng, Y.-X.; Ding, J. Chiral single molecule with biphenyl component exhibiting both TADF and RTP emissions enables highly efficient CP-OLEDs. *Angew. Chem., Int. Ed.* **2025**, *64* (40), No. e202512717.

(9) Wu, L.; Yuan, S.-W.; Wang, X.-Y.; Liu, C.; Yuan, X.-Y.; Tang, Y.-Y.; Zhang, Y.-W.; Xiao, X. Room-Temperature phosphorescent materials constructed based on Cucurbit[8]uril for encryption and anti-counterfeiting. *Spectrochim. Acta, Part A* **2025**, *343*, 126570.

(10) Uoyama, H.; Goushi, K.; Shizu, K.; Nomura, H.; Adachi, C. Highly efficient organic light-emitting diodes from delayed fluorescence. *Nature* **2012**, *492* (7428), 234−238.

(11) Hempe, M.; Kukhta, N. A.; Danos, A.; Batsanov, A. S.; Monkman, A. P.; Bryce, M. R. Intramolecular hydrogen bonding in thermally activated delayed fluorescence emitters: Is there evidence beyond reasonable doubt? *J. Phys. Chem. Lett.* **2022**, *13* (35), 8221−8227.

(12) Samanta, P. K.; Kim, D.; Coropceanu, V.; Brédas, J.-L. Up-conversion intersystem crossing rates in organic emitters for thermally activated delayed fluorescence: Impact of the nature of singlet vs triplet excited states. *J. Am. Chem. Soc.* **2017**, *139* (11), 4042−4051.

(13) Zhou, J.; Lin, J.; Guo, Z.; Xie, P.; Chen, C.; Mao, L. Tunable blue-light-emitting organic−inorganic zinc halides with thermally activated delayed fluorescence and room-temperature phosphorescence. *ACS Appl. Mater. Interfaces* **2024**, *16* (46), 63744−63751.

(14) Chen, R.; Guan, Y.; Wang, H.; Zhu, Y.; Tan, X.; Wang, P.; Wang, X.; Fan, X.; Xie, H.-L. Organic persistent luminescent materials: ultralong room-temperature phosphorescence and multi-color-tunable afterglow. *ACS Appl. Mater. Interfaces* **2021**, *13* (34), 41131−41139.

(15) Ji, W.; Pan, M.; Wu, H.; Ma, L.; Wang, Y. Stretchable polymer films doped with dual-emissive luminogens: dynamic afterglow, strain detection, and advanced anti-counterfeiting. *Adv. Opt. Mater.* **2025**, *13* (35), No. e02424.

(16) Zhang, X.; Qian, C.; Ma, Z.; Fu, X.; Li, Z.; Jin, H.; Chen, M.; Jiang, H.; Ma, Z. A class of organic units featuring matrix-controlled color-tunable ultralong organic room temperature phosphorescence. *Adv. Sci.* **2023**, *10* (3), 2206482.

https://doi.org/10.1021/acsapm.5c04339
ACS Appl. Polym. Mater. XXXX, XXX, XXX−XXX

(17) Ding, B.; Ma, X.; Tian, H. Recent advances of pure organic room temperature phosphorescence based on functional polymers. *Acc. Mater. Res.* **2023**, *4* (10), 827−838.
(18) Wu, H.; Shi, L.; Yang, C.; Wang, Y.; Wang, X.; Ma, L. Ultralong room-temperature phosphorescence of crystalline organic luminogens: excitation-dependence, chirality, and host-guest doping. *Spectrochim. Acta, Part A* **2026**, *344*, 126667.
(19) Yang, C.; Pan, M.; Ma, L.; Wang, Y. Three in one: one host−guest doping system with mechanochromism, long afterglow, and thermally activated delayed fluorescence. *Chem. Eng. J.* **2025**, *514*, 163205.
(20) Zhu, Y.; Wu, H.; Pan, M.; Ma, L.; Wang, Y. Achieving ultralong-lived flexible room-temperature phosphorescence, detection of strain and photostability, and high-level data encryption based on benzophenone derivatives. *Chem. Eng. J.* **2025**, *519*, 165087.
(21) Cui, J.; Ali, S. H.; Shen, Z.; Xu, W.; Liu, J.; Li, P.; Li, Y.; Chen, L.; Wang, B. ε-Polylysine organic ultra-long room-temperature phosphorescent materials based on phosphorescent molecule doping. *Chem. Sci.* **2024**, *15* (11), 4171−4178.
(22) Ma, D.-X.; Li, Z.-Q.; Tang, K.; Gong, Z.-L.; Shao, J.-Y.; Zhong, Y.-W. Nylons with highly-bright and ultralong organic room-temperature phosphorescence. *Nat. Commun.* **2024**, *15* (1), 4402.
(23) Hu, J.-H.; Hou, R.-X.; Liu, C.; Wang, Y.-P.; Liu, Y.-F.; Huang, Y.; Tao, Z.; Xiao, X. Ultra-long room temperature phosphorescent materials based on tetraphenylethylene derivatives for anti-counterfeiting and encryption applications. *Chem. Eng. J.* **2024**, *491*, 152177.
(24) Liang, H.; Yang, L.; Cheng, J.; Li, T.; Zhang, D.; Xu, Z. Stimuli-responsive recyclable polymers with room-temperature ultralong phosphorescence for anti-counterfeiting. *Adv. Funct. Mater.* **2026**, *36* (2), No. e13575.
(25) Liu, J.; Yao, J.; Mu, R.; Mao, X.; Li, H.; Sun, J.; Huang, J.; Feng, Q.; Cao, X.; Wang, J.; et al. N-B-N Isomer induced room temperature phosphorescence: expression, mechanistic insights, and multi-Level anti-counterfeiting applications. *Angew. Chem., Int. Ed.* **2025**, *64* (34), No. e202509104.
(26) Sun, W.; Shi, B.; Xia, Z.; Lü, C. Visible-light-excited long-lived organic room-temperature phosphorescence of phenanthroline derivatives in PVA matrix by H-bonding interaction for security applications. *Mater. Today Chem.* **2023**, *27*, 101297.
(27) Wang, D.; Gong, J.; Xiong, Y.; Wu, H.; Zhao, Z.; Wang, D.; Tang, B. Z. Achieving color-tunable and time-dependent organic long persistent luminescence via phosphorescence energy transfer for advanced anti-counterfeiting. *Adv. Funct. Mater.* **2023**, *33* (1), 2208895.
(28) Wang, M.; Li, F.; Lei, Y.; Xiao, F.; Liu, M.; Liu, S.; Huang, X.; Wu, H.; Zhao, Q. Excitation-dependent organic phosphors exhibiting different luminescence colors for information anti-counterfeiting. *Chem. Eng. J.* **2022**, *429*, 132288.
(29) Lei, Y.; Yang, J.; Dai, W.; Lan, Y.; Yang, J.; Zheng, X.; Shi, J.; Tong, B.; Cai, Z.; Dong, Y. Efficient and organic host−guest room-temperature phosphorescence: tunable triplet−singlet crossing and theoretical calculations for molecular packing. *Chem. Sci.* **2021**, *12* (19), 6518−6525.
(30) Liang, D.; Jia, J.-H.; Yang, M.; Cai, X.-B.; Yu, R.; Lu, C.-Z. Room-temperature phosphorescence enhanced by narrowing down ΔE_{ST} through tuning excited states energy levels. *Adv. Opt. Mater.* **2022**, *10* (20), 2201130.
(31) Liu, G.; Yue, L.; Wang, Y.; Xue, S.; Sun, Q.; Yang, W. Serial novel N-phenylcarbazole derivatives with two-in-one introduction of bromine and polar groups as hosts for efficient RTP and white emission regulation. *Chem. Eng. J.* **2024**, *498*, 155171.
(32) Song, S.; Sun, R.; Zeng, J.; Peng, X.; Tang, B. Z.; Zhao, Z. Exploring efficient purely organic room-temperature phosphorescence materials based on the heavy-atom effect of thioxanthone. *Adv. Opt. Mater.* **2025**, *13* (32), No. e02168.
(33) Sun, J.; Jia, J.; Zhao, B.; Yang, J.; Singh, M.; An, Z.; Wang, H.; Xu, B.; Huang, W. A purely organic D-π-A-π-D emitter with thermally activated delayed fluorescence and room temperature phosphorescence for near-white OLED. *Chin. Chem. Lett.* **2021**, *32* (4), 1367−1371.
(34) Tian, R.; You, J.; Yin, C.; Liu, Q.; Yan, C.; Wang, J.; Zhang, J.; Zhang, J. Organic ultralong room temperature phosphorescence materials with tunable responsiveness from cellulose. *ACS Appl. Polym. Mater.* **2025**, *7* (11), 6941−6950.
(35) Wang, Y.; Sun, Q.; Yue, L.; Ma, J.; Yuan, S.; Liu, D.; Zhang, H.; Xue, S.; Yang, W. Persistent organic white-emitting afterglow from ultralong thermally activated delayed fluorescence and room-temperature phosphorescence. *Adv. Opt. Mater.* **2021**, *9* (21), 2101075.
(36) Wu, X.; Peng, X.; Chen, L.; Tang, B. Z.; Zhao, Z. Through-space conjugated molecule with dual delayed fluorescence and room-temperature phosphorescence for high-performance OLEDs. *ACS Mater. Lett.* **2023**, *5* (3), 664−672.
(37) Xu, X.; Chen, P.; Xia, Y.; Hui, W.; Gao, H.; Luo, S.; Dai, W.; Zhong, J.; Lei, Y.; Chen, Y. Improving the phosphorescence properties of doped materials through the heavy atom effect of the hosts. *Mater. Chem. Front.* **2026**, *10*, 72−79.
(38) Zhou, Q.; Yang, C.; Zhao, Y. Dynamic organic room-temperature phosphorescent systems. *Chem* **2023**, *9* (9), 2446−2480.
(39) Zhan, L.; Chen, Z.; Gong, S.; Xiang, Y.; Ni, F.; Zeng, X.; Xie, G.; Yang, C. A simple organic molecule realizing simultaneous TADF, RTP, AIE, and mechanoluminescence: understanding the mechanism behind the multifunctional emitter. *Angew. Chem., Int. Ed.* **2019**, *58* (49), 17651−17655.
(40) Ji, W.; Pan, M.; Duan, J.; Ma, L.; Wang, Y. Boronic ester-functionalized dual-state emitter for oxygen/strain sensing and dynamic encryption. *Talanta* **2026**, *298*, 129058.
(41) Wu, X.; Ma, C.; Liu, J.; Liu, Y.; Luo, S.; Xu, M.; Wu, P.; Li, W.; Liu, S. In situ green synthesis of nitrogen-doped carbon-dot-based room-temperature phosphorescent materials for visual iron ion detection. *ACS Sustainable Chem. Eng.* **2019**, *7* (23), 18801−18809.
(42) Xia, Y.; Bai, Q.; Jiang, Y.; Li, Q.; Wang, D.; Xiao, X. Supramolecular self-assembly and metal−ligand-enhanced organic room-temperature phosphorescence for live cell imaging. *ACS Appl. Mater. Interfaces* **2025**, *17* (15), 22375−22383.
(43) Zhu, Y.; Pan, M.; Ma, L.; Wang, Y. The luminescence mechanism of two pure organic room temperature phosphorescent isomers, mechanical force detection, 3D modeling, and dynamic data encryption. *Chem. Eng. J.* **2025**, *505*, 159245.
(44) Wang, T.; Wang, X.; Yan, Q.; Zhang, K. Ultralong organic room-temperature phosphorescence modulated by balancing intramolecular charge transfer and localized excitation character of excited states. *Dyes Pigm.* **2024**, *224*, 112024.
(45) Wang, D.; Wu, H.; Gong, J.; Xiong, Y.; Wu, Q.; Zhao, Z.; Wang, L.; Wang, D.; Tang, B. Z. Unveiling the crucial contributions of electrostatic and dispersion interactions to the ultralong room-temperature phosphorescence of H-bond crosslinked poly(vinyl alcohol) films. *Mater. Horiz.* **2022**, *9* (3), 1081−1088.
(46) Wu, H.; Chi, W.; Chen, Z.; Liu, G.; Gu, L.; Bindra, A. K.; Yang, G.; Liu, X.; Zhao, Y. Room Temperature Phosphorescence: Achieving Amorphous Ultralong Room Temperature Phosphorescence by Coassembling Planar Small Organic Molecules with Polyvinyl Alcohol (Adv. Funct. Mater. 10/2019). *Adv. Funct. Mater.* **2019**, *29* (10), 1970063.
(47) He, M.; Tan, T.; Hou, H.; Guo, F.; Wang, X.; Li, Q.; Qu, L.; Wang, K.; Li, Y.; Yang, C. Construction of cross-linked polymer phosphorescence by functionalization of cyclotriphosphazene. *Adv. Opt. Mater.* **2025**, *13* (12), 2403164.
(48) Chen, H.; Zhang, Y.; Shan, J.; Dong, M.; Qian, Z.; Lv, A.; Qian, H.-J.; Ma, H.; An, Z.; Gu, L.; et al. Water-resistant organic room-temperature phosphorescence from block copolymers. *Angew. Chem., Int. Ed.* **2025**, *64* (17), No. e202500610.
(49) Zhu, S.; Xu, B.; Luo, T.; Li, H.; Wu, X.; Zheng, S.; Li, H.; Gao, Y.; Zhang, K. Organic afterglow vesicles. *Adv. Sci* **2026**, *13*, No. e23635.

https://doi.org/10.1021/acsapm.5c04339
ACS Appl. Polym. Mater. XXXX, XXX, XXX−XXX